A6,10-C1.7,6,x42812r

Rapid Modeling of Electrostatic Forces and Torques Considering Dielectrics

Joseph Hughes[a*], Hanspeter Schaub[b]

[a] *Department of Aerospace Engineering, University of Colorado at Boulder, 429 UCB, Boulder, CO, 80309, Joseph.Hughes@Colorado.edu*

[b] *Department of Aerospace Engineering, University of Colorado at Boulder, 429 UCB, Boulder, CO, 80309, Hanspeter.Schaub@Colorado.edu*

* Corresponding author

Abstract

Spacecraft can charge naturally to 10s of kiloVolts in Geosynchronous orbit due to their interactions with the space plasma and the sun. This charging can cause forces and torques that can perturb the orbits of uncontrolled debris objects or be used as a form of touchelss actuation in an active charging multi-craft formation. Prior work for electrostatic force and torque prediction has developed rapid and accurate methods for conducting spacecraft using the Multi-Sphere Method (MSM). This paper extends MSM for spacecraft composed of conductors and dielectrics. It is found that for some spacecraft and charging regimes dielectrics can be neglected without introducing significant errors. For the cases that require dielectrics be considered, MSM is augmented to include dielectric point charges as well as conducting spheres that are placed and sized by a numerical optimizer. Designs are developed that perform better than an average of 2% error for all spacecraft and charging scenarios considered.

Keywords: Space Debris, Dielectrics, Electrostatics,

1. Introduction

In the Geosynchronous Earth Orbit (GEO) regime, satellites charge to very high voltages sometimes as dramatic as -19 kV [1]. This charging causes small forces and torques on the body due to interactions with earth's magnetic field, which changes the orbits of some uncontrolled lightweight debris objects through the Lorentz force [2, 3, 4, 5]. If nearby spacecraft use active charging such as electron and ion guns, larger forces and torques are felt between the crafts. This enables novel Coulomb formation flying missions [6, 7, 8]. These forces can also be used for touchless re-orbiting of GEO debris to its graveyard orbit in a matter of months using the Electrostatic Tractor (ET) [9]. If a spacecraft has a non-symmetric charge distribution, it also experiences torques which can be harnessed for touchless de-spin before servicing or grappling [10, 11, 12].

There are many separate challenges to electrostatic actuation such as prescribing the appropriate electron and/or ion beam current and voltage, sensing the voltage, position, and attitude of a passive space object, and designing control laws that perform well for either tugging or de-spinning. In order to design and implement stable and performant control laws in any of the above mission scenarios, accurate and fast methods are needed to predict the force and torque on both spacecraft using only in-situ measurements such as the voltage of each craft, and their relative separation and attitude. Accuracy is important because under or over prediction can seriously harm performance, or lead to a collision [13]. Speed is important because the force and torque must be predicted in real time by the flight computer. This paper discusses how to predict electrostatic force and torque for a body that is composed of conductors and dielectrics as shown in Fig. 1.

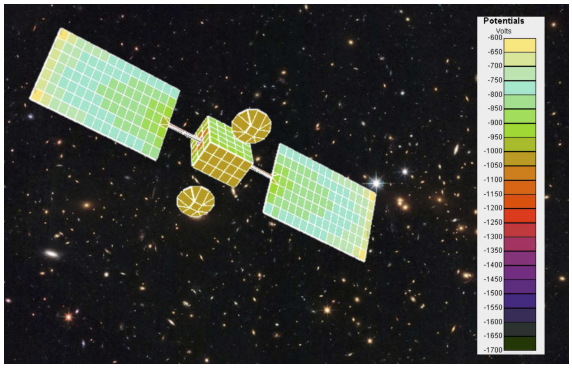

Fig. 1. Voltages of a spacecraft with conducting and dielectric surfaces. Computation done in NASCAP-2k

There are many methods for force and torque prediction ranging from very accurate but much slower than realtime methods such as Finite Element Analysis (FEA), or faster and more scalable methods such as the Method of Moments (MoM) [14] or Boundary Element Method (BEM). Prior work explores using the Galerkin method to model forces between two dielectric spheres [15]. A relatively new scheme for electrostatic force and torque prediction is the Multi-Sphere Method (MSM) [16]. MSM is very similar to the MoM in that an elastance matrix is popu-

lated and then inverted to find the charge distribution. The Coulomb force is applied from every discretized charge on one body to every discretized charge on the other body. MSM differs from MoM in that the elements of the elastance matrix are tuned to match force and torque created by a higher-fidelity method rather than from first principles. Because of this tuning, MSM can predict forces and torques with only a few percent error using only 3-4 spheres for a two craft system [17, 18], but requires a truth model from which to optimize. It is a robust method for force and torque prediction for conducting systems, however, not all spacecraft are continuously conducting. Recent work [19] investigates how to modify MSM to account for dielectrics and finds very small impacts when the dielectric lays directly on top of the conducting surface of the spacecraft.

Most spacecraft are built to be continuously conducting to avoid differential charging and arcing. However, some of the conducting covering may degrade with time and lose its conductivity. Two scenarios where this may occur is the coverglass coating on the solar panels and the Multi-Layer Insulation (MLI). Solar panels require a glass cover to protect from proton radiation, and there is usually a conductive clear coating over the glass, however, this coating may degrade or flake off and can leave sections of the non-conductive glass exposed. MLI also usually has a gold or aluminum coating, but this may flake off or otherwise degrade. Additionally, some spacecraft are not built fully conducting to begin with, and will have large dielectric portions. In the case of coverglass and MLI, there is a thin layer (10-100 μm) of dielectric sitting directly on top of a conductor connected to spacecraft ground. However, in an effort to save weight, some spacecraft have MLI wrapped around a skeleton frame with very little area of the MLI touching the conducting bus.

2. Problem Statement

The Multi-Sphere Method (MSM) was originally created as a fast way to predict the electrostatic force and torque between conductors [16]. It is very similar to the Method of Moments, but rather than the elements of the elastance matrix being derived from first principles, they are hand-tuned to match force, torque, or E fields predicted by a higher fidelity model like FEA or MoM.

As shown in Figure 2, MSM approximates a spacecraft as a collection of spheres with variable positions and radii. The voltage on any sphere is a function of both its own charge and the charge of all nearby spheres. If these spheres are far enough away to be approximated as point charges, the voltage is given by: [16]

$$V_i = \frac{1}{4\pi\epsilon_0}\frac{q_i}{R_i} + \sum_{j=1,\, j\neq i}^{n} \frac{1}{4\pi\epsilon_0}\frac{q_j}{r_{i,j}} \tag{1}$$

Where q_i and R_i are the charge and radius of the i^{th} sphere, respectively, $\rho_{i,\,j}$ is the center-to-center distance between spheres i and j, and ϵ_0 is the permittivity of free space constant. If the voltages of each sphere are given by $\boldsymbol{V} = [V_1, V_2, ...V_n]^{\mathrm{T}}$ and the charges are given by $\boldsymbol{q} = [q_1, q_2, ...q_n]^{\mathrm{T}}$, the relationship between the two is

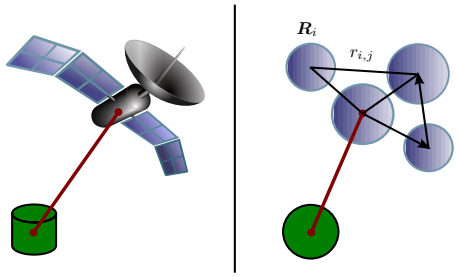

Fig. 2. Multi-Sphere Method concept

$$\boldsymbol{V} = [S]\boldsymbol{q} \tag{2}$$

where $[S]$ is the elastance matrix defined below:

$$[S] = \frac{1}{4\pi\epsilon_0}\begin{bmatrix} 1/R_1 & 1/r_{1,2} & \cdots & 1/r_{1,n} \\ 1/r_{2,1} & 1/R_2 & \cdots & 1/r_{2,n} \\ \vdots & \vdots & \ddots & \vdots \\ 1/r_{n,1} & 1/r_{n,2} & \cdots & 1/R_n \end{bmatrix}\begin{bmatrix} q_1 \\ q_2 \\ \vdots \\ q_n \end{bmatrix} \tag{3}$$

If the voltage is known, the linear system can be solved for the charges $\boldsymbol{Q}$. Combining the charges with the locations of the spheres allows the force and torque to be computed. In a flat E field the net force and torque are

$$\boldsymbol{F} = \boldsymbol{E}\sum_{i=1}^{n} Q_i \qquad \boldsymbol{L} = \sum_{i=1}^{n} Q_i\boldsymbol{\rho}_i \times \boldsymbol{E} \tag{4}$$

for an MSM model with n spheres where $\boldsymbol{\rho}_i$ points from the origin to sphere i. In a de-tumbling scenario another spacecraft (with m spheres) is nearby and the Coulomb force is applied between each pair of spheres:

$$\boldsymbol{F} = \sum_{i=1}^{n}\sum_{j=1}^{m} \frac{Q_i Q_j \boldsymbol{r}_{ij}}{4\pi\epsilon_0 r_{ij}^3} \tag{5}$$

The torque is then:

$$\boldsymbol{L} = \sum_{i=1}^{n}\sum_{j=1}^{m} \boldsymbol{\rho}_i \times \frac{Q_i Q_j \boldsymbol{r}_{ij}}{4\pi\epsilon_0 r_{ij}^3} \tag{6}$$

This process has been used successfully for modeling spacecraft with complex geometries as close as a few craft diameters with errors of a few percent [18].

This paper will investigate two separate questions. First, under what circumstances do dielectrics have to be

accounted for to accurately model the force and torque? Second, how can MSM be modified to account for dielectrics? To answer the first question four different template spacecraft are considered under three different charging scenarios. Once situations that require modeling the dielectric effects are identified, a modification to conducting MSM is presented and tested on the template spacecraft.

3. Method of Images Analysis

To gain some analytical insight into the first question of when dielectrics need to be accounted for, first consider a much simpler system using the Method of Images (MOI) [20, 21, 22]. If a positive point charge is held a distance z above a grounded infinite conducting plate, a negative induced charge will pool up beneath the point charge due to attraction. For the purposes of calculating the field above the plate, one can assume that there is a negative charge of equal magnitude z below the plate. In this situation, net charge is zero because the conductor "canceled out" the point charge.

If a finite sphere is considered rather than an infinite plate, the induced charge q' becomes smaller and moves closer to the surface. For a sphere with radius R, the induced charge is given by

$$q' = -\frac{R}{R+d}q \tag{7}$$

where d is the distance between the dielectric charge and the surface of the conductor, and Q_D is the dielectric charge as is shown in Fig. 3. When d is much smaller than R, the induced charge is nearly equal and opposite to the dielectric charge and will cancel out its effect on the total charge. However, when d is comparable to R, the effect of the dielectric charge on the total charge is much more significant.

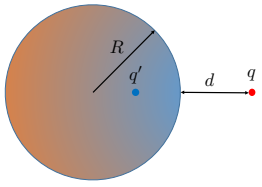

Fig. 3. Method of Images concept illustration

There are many differences between the electric field in the vicinity of a point charge and conducting sphere, and the electric field in the vicinity of a charged solar panel and conducting spacecraft bus, but there is still some intuition to gain from this simple analysis. The MOI predicts that when the dielectric is very near the conductor, its charge will be mostly canceled out regardless of how charged it is. Dielectric coatings sitting directly over conductors will likely not cause any significant changes for this reason. If the dielectric is far from a conductor, like a solar panel might be, then the effects are more significant. To understand how this simple principle applies to more complex spacecraft, numerical studies are performed next.

4. Truth Model Development

The Method of Moments (MoM) is used to create a truth model of the electric field in the vicinity of the spacecraft for a simpler MSM model to match. Prior work [18] has found that MSM models that match the E field also match the force and torque very well, and matching E fields solves a number of other optimization issues as well.

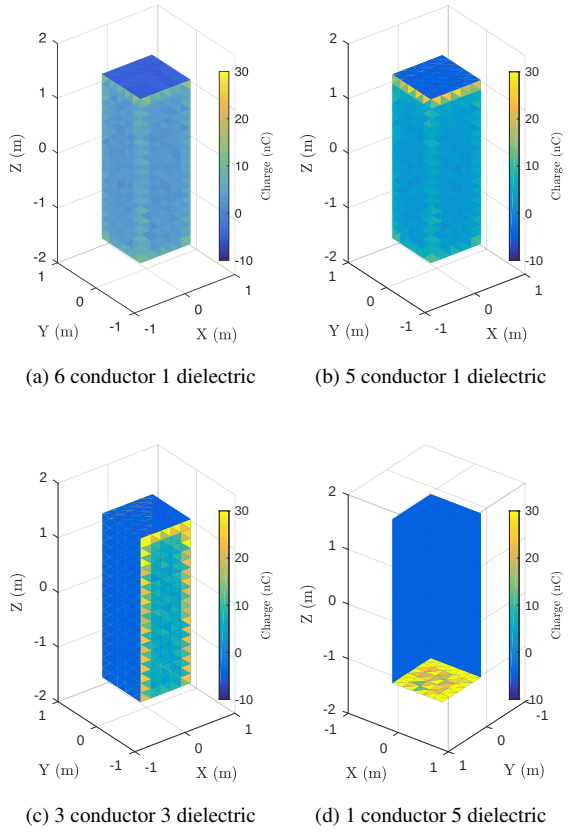

(a) 6 conductor 1 dielectric

(b) 5 conductor 1 dielectric

(c) 3 conductor 3 dielectric

(d) 1 conductor 5 dielectric

Fig. 4. Four template spacecraft truth models computed using the Method of Moments

This is done for four spacecraft under three separate charging conditions. The first spacecraft (Fig 4a) is a 3 m by 1 m box with a dielectric hovering 25.4 μm ($\sim$1 mil) above the top of the spacecraft. This serves as a model of the case where the MLI is stretched over the conducting exterior of the spacecraft. The small displacement off the surface is chosen to be a common thickness for MLI. The second spacecraft (Fig. 4b) is almost identical to the first but the top conductor is removed and the dielectric

is shifted down to be flush so that it is stretched over the perimeter of the conductor like the surface of a drum. The third spacecraft (Fig. 4c) has three panels made of dielectric so that it has equal area of conductor and dielectric. The fourth and final spacecraft (Fig. 4d) is composed of 5 dielectric panels and a single conducting panel on the very bottom. All spacecraft are referred to with the shorthand "XcYd" where X is the number of conducting panels and Y is the number of dielectric panels, so the last spacecraft discussed can be indicated by 1c5d. These four spacecraft span the range from a small amount of dielectric completely on top of a conductor to almost all dielectric with very little conductor very far away.

In all subplots in Fig. 4 the conductor is charged to +30 kV and the dielectric to -250 nC/m^2. For some models (especially the 1c5d one), the peak charge per element goes up to 94 nC, but the color scale only extends up to 30 nC per element to better show the charge distribution. The positive charge concentrates near the negative dielectric in all cases. Consider the first two cases (Fig. 4a and Fig. 4b) which only differ by the inclusion of a conductor backing behind the dielectric. In the case without the backing, much more charge must accumulate on the side panels to cancel out the negative charge, while in the case with the backing all the charge accumulates on that backing and is not seen. The other two cases (Fig. 4c and Fig. 4d) have even more positive charge accumulate to cancel out the large negative panels.

In addition to solving for the charge distribution, the electric field in the vicinity of the spacecraft is also found. The E field is computed at 30 points uniformly spread across each of 12 different spherical shells ranging in radius from 3 to 25 meters. The E field is computed for 3 different cases as well - the first in which only the conductor is charged to +30 kV and the dielectric has no net charge (but has a high voltage due to its proximity to the dielectric), one in which the conductor is charged and the dielectric is additionally charged to -250 nC/m^2, and the last in which the conductor is grounded (0 V) and the dielectric is charged. These 30 points per shell across 12 different shells for 3 different charging scenarios for 4 different spacecraft represent 4320 individual E field computations.

5. Conductor Solutions

As a first attempt at modeling these spacecraft, the dielectric surfaces are ignored entirely and the optimization is done using a dataset where the dielectric is uncharged. This method has promise for the spacecraft with dielectrics close to conductors such as the 6c1d because of the image charges. A 3 sphere MSM model where all spheres are constrained to stay on the z axis, but can change their height and radius is optimized using only the conducting data for all spacecraft. The cost function is the average percent error of the E field the MSM model produces relative to the truth model. The final solution for the 3c3d spacecraft is shown in Fig. 5 with its three spheres constrained along the z axis. Since all three spheres have a tunable radius and height, there are 6 free parameters in this model.

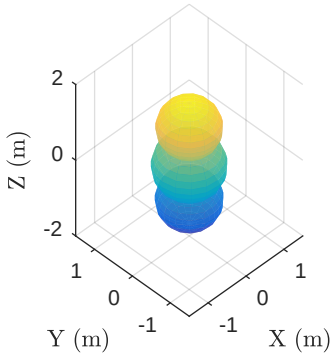

Fig. 5. Optimal MSM model for 3c3d spacecraft ignoring dielectrics

This process of ignoring the dielectrics is applied to all four spacecraft and their performance in both the conducting and mixed charging regimes is shown in Fig. 6. All MSM models have only conducting spheres and are optimized using just the conducting dataset (+30 kV and no dielectric charge).

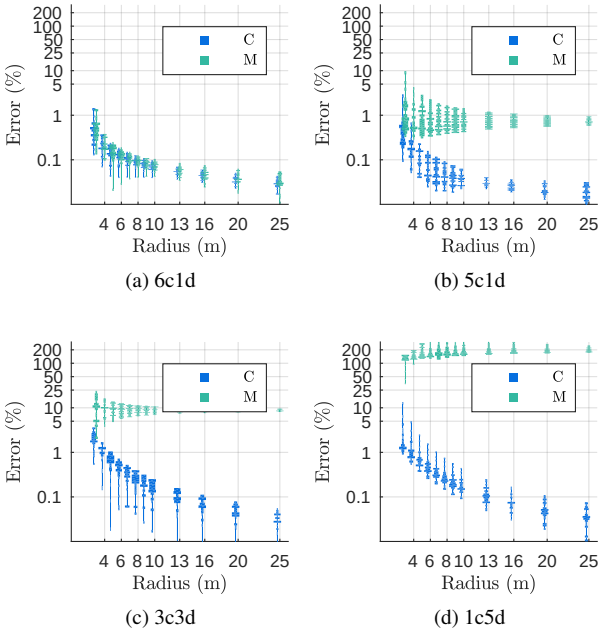

(a) 6c1d (b) 5c1d

(c) 3c3d (d) 1c5d

Fig. 6. Performance of a conductor-only MSM model in pure conducting (C) and mixed (M) charging regimes

The performance of the 6c1d model is shown using a violin plot in Fig. 6a. Violin plots are a good way to show a lot of data at once; they essentially show multiple histograms rotated by 90°. The width of each bar corresponds to the number of cases in the bin shown on the y axis for the case shown on the x axis. In the following violin plots, the cases correspond to how far away the E field is measured, the bins correspond to the percentage error (with reference to the MoM truth model), and the color corresponds to the charging scenario, with the dark blue being the conductor, (C) and the aqua being the mixed case (M). For the 6c1d spacecraft (Fig. 6a), the errors for the C and M case are incredibly similar, and both very good - they are almost always below 1% error, and after 10 m they are always better than 0.1% error. They are similar because the induced charge on the top plate of the conductor almost entirely cancels out the dielectric charge, making it as though the charged dielectric is not even there.

Moving to the 5c1d case (Fig. 6b), the conducting regime errors are almost unchanged, but the mixed charging regime errors are larger. This is because the two cases are no longer as similar due to the lack of a top conducting panel to cancel out the dielectric charge. Despite this, the conductor only model has only a few percent error in the M category, which is more than accurate enough for many missions. The 3c3d spacecraft (Fig. 6c) is slightly harder to model with mixed regime errors in the 10% range even though conductor errors are still very small. This is because much of the dielectric is much farther away from the conductor. Moving finally to the 1c5d case (Fig. 6d), the C errors are still very good, but the M errors have increased up to 200% error.

From this analysis, it seems that one would not bother to model dielectrics for the 6c1d or the 5c1d, but probably the 3c3d and definitely for the 1c5d. To expand this analysis to more continuous charging conditions, the dielectric charge density is swept from 1 - 1000 nC/m and voltage from 10V to 100 kV for each spacecraft. For each charging condition, compute the charge percentage error as $100\,(Q_C - Q_T)/(Q_T)$ where Q_C is the total charge found if the dielectric is ignored and Q_T is the true total charge. This charge error correlates with the percentage error when computing force in the far field, and should be small to ensure accuracy. The charge error is always 100% when the voltage is zero because the conductor only solution will always predict $Q_C = 0$, even if the total charge Q_T is negligible. Thus, this method for judging the charge error can produce misleading results when the voltage is small. The charge errors are shown in Fig. 7 where the different colors indicate different spacecraft.

In general, the charge errors grow as the dielectric charge is increased, which makes sense as the ignored charge becomes larger. The charge errors are also large when the voltage is low because they are percentage based.

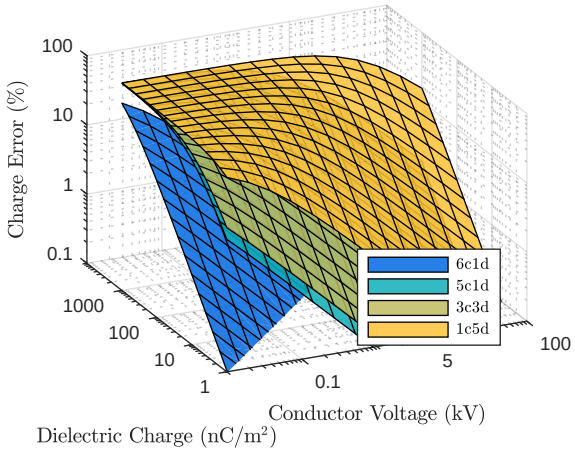

Fig. 7. Charge error as a function of voltage and dielectric charge density for four spacecraft

The 1c5d spacecraft has the worst errors, as expected since it is mostly dielectric, and has many panels which do not come close to the conductor. For this template spacecraft, errors will be large for almost all dielectric and conductor charge configurations. For the two intermediate spacecraft - the 3c3d and 5c1d, the performance is very similar. They both have charge errors larger than 10% if the dielectric charge is larger than 500 nC/m^2 when the voltage is 5 kV. The 6c1d spacecraft is the bounding case - neglecting dielectrics only introduces errors when the spacecraft is at very low voltages, at which the actual charge and resulting force and torque will be very small.

This manner of analysis can be used to quickly check if dielectrics ought to be considered in an analysis. First the self and mutual dielectric capacitances are found for the spacecraft in question. Next the voltage and dielectric charge ranges are found, and finally the charge error is computed for the voltage and dielectric charge ranges. If the charge error is higher than the acceptable error for that mission, dielectrics must be included. This answers the first question "when ought dielectrics to be considered?" Now, how best to model dielectrics is considered.

6. Dielectric MSM Methodology

Dielectrics charge on much slower timescales than conductors because of their large mutual capacitance. Because of this, they are treated as known point charges rather than a known voltages. To modify conducting MSM to include dielectrics, the model is broken into two parts for the conductor and dielectric:

$$\begin{bmatrix} \boldsymbol{V}_C \\ \boldsymbol{V}_D \end{bmatrix} = \begin{bmatrix} S_C & S_M \\ S_M^T & S_D \end{bmatrix} \begin{bmatrix} \boldsymbol{Q}_C \\ \boldsymbol{Q}_D \end{bmatrix} \tag{8}$$

where the C and D subscripts denote conductor and dielectric respectively, and the M is for mutual. Since the

voltage of the conductor and the charge of the dielectric are assumed known and the charge distribution for the conductor is sought, the top line of this equation is rearranged to give

$$\boldsymbol{Q}_C = [S_C]^{-1}(\boldsymbol{V}_C - [S_M]\boldsymbol{Q}_D) \tag{9}$$

Then the total charge $\boldsymbol{Q}$ can be formed as $\boldsymbol{Q} = [\boldsymbol{Q}_C, \boldsymbol{Q}_D]^T$. The force, torque, or E field are then computed as discussed in the earlier section.

When modeling conducting bodies, the MSM optimization problem is fairly simple - change the position and size of the spheres to best match the force, torque, or E field from a truth model. With dielectrics, there are a few changes - now there are both conducting spheres and point charges which may be moved, and there are many different charging scenarios to consider when producing the truth model. With conductors, it does not matter what voltage is chosen for the truth model, as long as it is not zero. With dielectrics included, models that work well for a high voltage case can perform very poorly for a high charge case.

To address the problem of optimizing for just one charging regime, three charging scenarios are included in the truth file; one with just the conductor charged and no charge on the dielectric, one with both conductor and dielectric charged, and one with just the dielectric charged. Because using many point charges does not greatly slow down computation time, and to make the optimization easier, the point charges are uniformly distributed over the dielectric panels. This scheme is shown in Fig. 8.

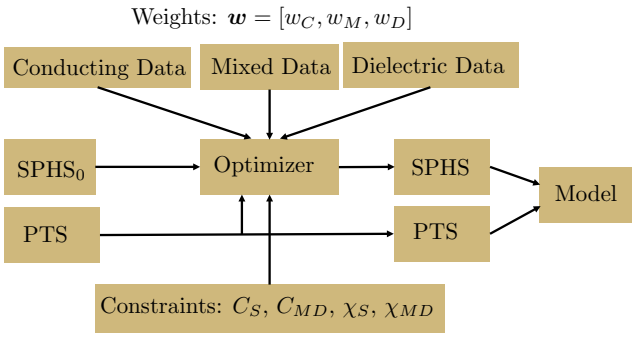

Fig. 8. Optimization scheme for dielectric MSM

An initial guess for the spheres location and radius is supplied to the optimizer. The optimizer uses the points model along with the spheres model to compute the E field at all 30 points in all of the 12 shells for all 3 charging scenarios. The cost is computed from the average percentage error for all three charging scenarios and the weights. A selection of constrains, discussed later, can also be used to ensure behavior in the far field. The final spheres model is combined with the prescribed points model to make the full model for that spacecraft.

7. Optimization Constraints

Prior work in optimizing MSM models for conductors [17, 18] has shown that enforcing that the MSM model have the same self capacitance as the object being modeled can make the optimization more robust and also provides a guarantee of correctly modeling the force in the far field. The self capacitance is a scalar parameter that determines how much charge is present at a given voltage. For a spacecraft with both dielectric and conducting components, the total charge is a function of both the conductor voltage and the dielectric charge. The total charge is the sum of the dielectric charge and the conductor charge:

$$Q = \mathbb{1}_{n_C}^T \boldsymbol{Q}_C + \mathbb{1}_{n_D}^T \boldsymbol{Q}_D \tag{10}$$

where the notation $\mathbb{1}_n$ indicates a column vector of ones with n elements and n_C and n_D denote the number of conducting and dielectric elements. Now substitute in Eq. (9) for $\boldsymbol{Q}_C$ and rearrange:

$$\begin{aligned} Q &= \mathbb{1}_{n_C}^T [S_C]^{-1}(\boldsymbol{V}_C - [S_M]\boldsymbol{Q}_D) + \mathbb{1}_{n_D}^T \boldsymbol{Q}_D \\ &= C_S V_C + C_{MD} Q_D \end{aligned} \tag{11}$$

where the self capacitance C_S and mutual dielectric capacitance C_{MD} are defined as

$$C_S \equiv \mathbb{1}_{n_C}^T [S_C]^{-1} \mathbb{1}_{n_C} \tag{12}$$

$$C_{MD} \equiv (1 - \mathbb{1}_{n_C}^T [S_C]^{-1} [S_M] \mathbb{1}_{n_D}^T / n_D) \tag{13}$$

The self capacitance determines how sensitive the total charge is to the voltage on the conductor, and the mutual dielectric capacitance determines how sensitive the total charge is to the dielectric charge. If $C_{MD} = 1$, then adding charge to the dielectric adds exactly that much to the total charge. If $C_{MD} = 0$, then adding charge to the dielectric adds no charge at all to the total charge because the induced charge cancels it out. Referencing back to the MOI solution $C_{MD} \approx 1 - R/(R+d)$. So when the dielectric is close to the conductor ($d << R$), C_{MD} will be close to zero, and the dielectrics will have minimal effects. When the dielectric is far from the conductor ($d \sim R$), C_{MD} will be close to one and dielectrics will play a larger role. Unlike the self capacitance which has units of Farads, C_{MD} is dimensionless and is always between 0 and 1.

The total charge is 0th order moment of the charge distribution. The first order moment of the charge distribution is the dipole ($\boldsymbol{q}$). The dipole is a 3×1 vector formed by multiplying the total charge by a vector pointing from the center of the coordinate system (usually at the center of mass) to the center of the charge and is discussed in greater detail in Reference [23]. MSM models that match the total charge and the dipole will correctly predict the torque as well as the force in the far field.

For a MSM model with both dielectric and conducting parts, the dipole is a combination of the dipole from both

the dielectric and conducting portions:

$$\boldsymbol{q} = \boldsymbol{\chi}_S V + \boldsymbol{\chi}_{MD} Q_D \tag{14}$$

where the parameters $\boldsymbol{\chi}_S$ and $\boldsymbol{\chi}_{MD}$ are the self and mutual susceptibilities defined by:

$$\boldsymbol{\chi}_S \equiv [R_C][S_C]^{-1}\mathbb{1}_{n_C} \tag{15}$$

$$\boldsymbol{\chi}_{MD} \equiv \frac{[R_D]\mathbb{1}_{n_D}}{n_D} - \frac{[R_C][S_C]^{-1}[S_M]\mathbb{1}_{n_D}}{n_D} \tag{16}$$

where $[R_C]$ and $[R_D]$ are matrices containing the location of every sphere/point in an MSM model or the centroid of every triangle in a MoM model for both the conductor and dielectric:

$$[R] = \begin{bmatrix} x_1 & \dots & x_N \\ y_1 & \dots & y_N \\ z_1 & \dots & z_N \end{bmatrix} \tag{17}$$

The self susceptibility determines how sensitive the total dipole is to the conductor voltage, and the mutual susceptibility determines how sensitive it is to the dielectric charge. If the mutual susceptibility is small, the charge on the dielectric will not influence the dipole strongly. Once again the units differ because the two susceptibilities multiply different quantities.

These four parameters, C_S, C_{MD}, χ_S, and χ_{MD}, are all intrinsic and unchanging properties of a given spacecraft geometry. These constraints are enforced during optimization to understand how they affect the performance. Since these four constrains can be enforced in groups, there are 16 different unique sets of constraints that can be used. For each constraint set, the MSM solution is optimized for the 3c3d spacecraft using a prescribed points model for the dielectric which uses 36 points and a seven sphere MSM model which has 3 spheres on each of the conductor panels and one along the central axis.

The results are shown in Fig. 9. The MSM solution for one of the 16 cases is shown in Fig. 9a. This particular optimization was constrained to match the self capacitance and self susceptibility, but not either of the mutual terms. The performance of this model is shown as a triple violin plot in Fig. 9b. The errors for all three scenarios decreases with distance, dropping below 1% at around 10 m for the dielectric case and near 7 m for the conductor and mixed case. The maximum error is near 10% but that is only for the dielectric only case at the closest distance. Since it would be tedious to show a triple violin plot for each of the 16 different constrain cases, the performance is reduced to two scalar values - first the cost function which is the mean of the errors for each field point at each radius and each charging condition. This value is shown for all of the 16 constraint cases in Fig. 9c.

The first thing to notice is that the errors are all very good regardless of the constraints used. The maximum mean error is 1.35%, which is less than all the other uncertainties in the system are likely to be. The lowest error is found with no constrains at all, which is expected as the optimizer has access to more solutions than the constrained solutions. In general, the leftmost and third-from-left columns are similar to each other and darker than the rest, indicating that the optimizer picks MSM models that match self capacitance even if that constraint is not enforced. The first and third rows also have lower error than the other rows, especially when combined with the first and third columns. This indicates that C_S and $\boldsymbol{\chi}_S$ are the most important parameters to match. Looking at the outside edge near the upper left corner shows the effects of including just one constraint at a time. No constraints at all gives a mean error of 1.11 %, just $\boldsymbol{\chi}_S$ gives 1.14 %, $\boldsymbol{\chi}_{MD}$ gives 1.16 %, C_{MD} gives 1.17 %, and C_S gives the same 1.11%. This analysis of looking at the constraints one at a time supports the idea that C_S and $\boldsymbol{\chi}_S$ are the most important parameters to match.

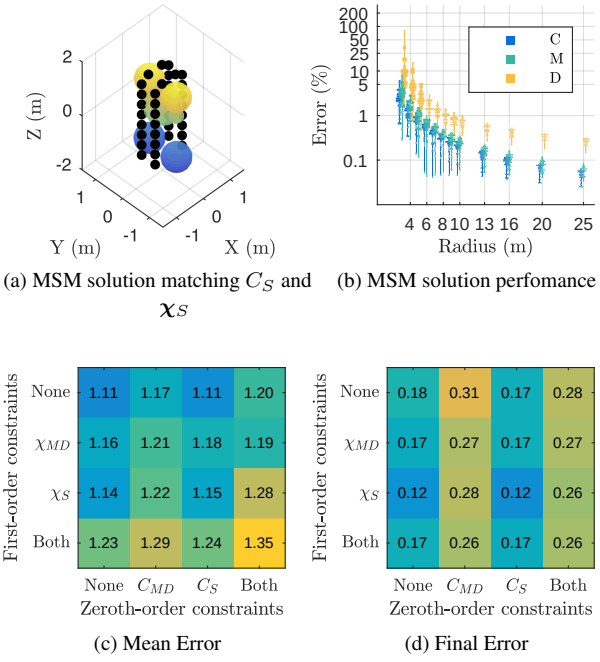

(a) MSM solution matching C_S and $\boldsymbol{\chi}_S$

(b) MSM solution perfomance

(c) Mean Error

(d) Final Error

Fig. 9. Effects of enforcing constraints

The second scalar value to draw from the violin plots is the mean error for all charging conditions at 25 meters. This final error should be more sensitive to enforcing constraints due to its distance and is shown in Fig. 9d. The first and third column are even more dramatically better than the rest than in the mean error, as is the third row. Here, the lowest error comes from enforcing the self susceptibility constraint either with or without the self capacitance. The mean and final error analysis both show that C_S and $\boldsymbol{\chi}_S$ are the most important constraints to enforce

for this spacecraft. Enforcing both only hurts the mean error by 0.04%, and provides a guarantee of performance in the far field.

This particular seven sphere, 36 point model has 8 free parameters, which makes it possible to enforce any combination of constraints and still have many free parameters to tune for optimality. Despite this, it is still a very difficult optimization requiring very precise initial conditions. For more simple MSM models with fewer free parameters, it is not possible to enforce all of these constraints depending on the number of free parameters. It is also possible that the constrains are not compliant for some MSM models — for example a MSM model that had all spheres constrained on the z axis would never be able to match any non-zero x and y components of $\boldsymbol{\chi}_S$. For this model, constraints aid the solution since they are compliant. For other models, they are detrimental or impossible to enforce.

8. Performance and Time Analysis

The earlier section investigated the effect of constraints while keeping the model (3c3d spacecraft with 7 spheres and 36 points) constant. This section uses no constraints, but investigates the E field fitting performance while changing the spacecraft and its sphere and points model. For all spacecraft, the points are distributed equidistantly across the dielectric panels as shown in Fig. 9a. This model has two rows which results in 36 points, one row gives in 11 points while 3 rows will give 75 points. For dielectric-heavy spacecraft (such as the 1c5d) there are naturally many more points than for conductor-heavy spacecraft (such as the 6c1d).

For all spacecraft, the spheres model uses a few spheres placed either along the z axis or in the plane of the conducting panels. The simplest model uses two spheres where both spheres have variable radii and position along the z axis. The next most complicated model has 3 spheres with variable radii and height for 6 total parameters. More advanced models have one sphere free to move along the z axis and a few rings of spheres centered on the panels that can change height and radius. Fig. 9a shows a model for the 3c3d spacecraft with three rings of spheres along the vertical panels and one central sphere along the z axis for a total of seven spheres. For the 1c5d spacecraft, none of the above models work well, so 1, 4, and 5 sphere models are made which keep all spheres in the $z = -1.5$m plane. In total, 10 separate sphere and 9 separate point models are considered for a total of 53 optimizations which are shown in Fig. 10. If no points are used, the dielectric dataset is ignored because it will always give 100% error.

The first plot (Fig. 10a) shows how well different designs model the E field surrounding the 6c1d spacecraft. Earlier analysis found that dielectrics did not need to be modeled, and this analysis confirms that and additionally finds that that adding points actually hurts the solution. If no points are used, the mean errors are all less than 0.2%,

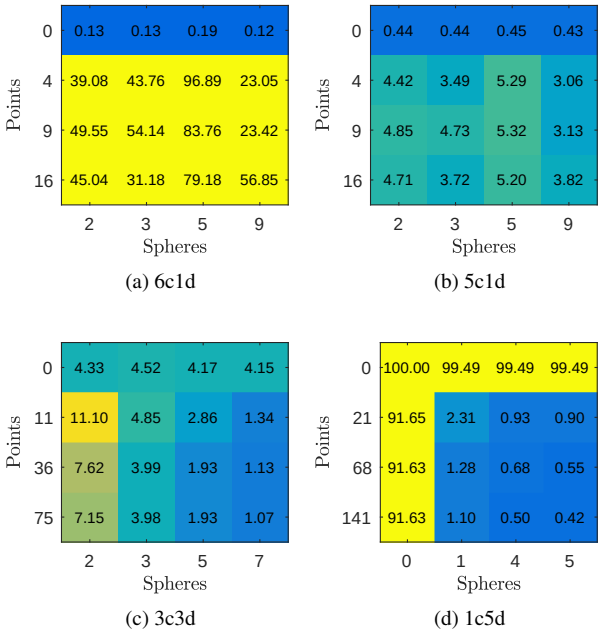

(a) 6c1d (b) 5c1d

(c) 3c3d (d) 1c5d

Fig. 10. Mean error of E field fitting for different sphere and point models

but if points are added they jump up to at least 20% and sometimes almost 100%. Among the conductor-only solutions, there is very little variation, with more spheres helping in general except for the 5 sphere model.

Moving to the 5c1d spacecraft (Fig. 10b), adding points still makes the solution worse but not by as much as the 6c1d. Ignoring the dielectric gets errors near 0.5%, but including them gets errors near 5%. In general, more spheres helps, with the exception of the 5 sphere model, which appears to be an all-around bad model regardless of the number of points used on both the 6c1d and 5c1d spacecraft. For both of these spacecraft, one ought to ignore the dielectrics entirely.

The 3c3d spacecraft (Fig. 10c) has equal area of conductor and dielectric and has slightly smoother behavior. Ignoring dielectrics results in mean errors near 4%, and including them can either help or hurt this solution. For instance, including points makes the solution nearly 3 times worse for a two sphere model, but nearly 3 times better for a 7 sphere model. For any models with more than 3 spheres, dielectrics ought to be included. Except for the first row, more spheres and points both help the solution. Since the columns are more distinct than the rows, one can conclude that the number of spheres is more important than the number of points, although the jump from 0 to 11 and 11 to 36 points is significant.

Finally, the 1c5d spacecraft mean error is shown in Fig. 10d. Since this spacecraft is virtually all dielectric, a points only solution is also considered. Both the points

and only spheres cases preform poorly with errors near 100%. For the cases with both spheres and points, the errors are much better, and decreases as spheres and points are added. In contrast to the 3c3d spacecraft, the rows are just as distinct as the columns, which indicates that adding points for this spacecraft is more valuable than on the 3c3d, which makes sense since the dielectric is larger and plays a larger part in the E field.

Overall, the two spacecraft for which dielectrics ought not be included are the easiest to model with errors always less than 0.5%. The 3c3d spacecraft provides an intermediate case where the number of spheres being used determines whether points ought to be used. For all spacecraft, a model exists which keeps the average error below 1.5%, which is likely lower than other errors expected in the system.

Many of the proposed applications of electrostatic force modeling must evaluate quickly as well as accurately. To investigate the trade space between accuracy and time, the number of arithmetic operations needed is found. For an MSM model with n conducting spheres and m dielectric point charges, the number of operations N required to find the charge at each node (using Eqn. (9)) is

$$N = \frac{2}{3}n^3 + \frac{11}{2}n^2 - \frac{25}{6}n + 2mn \tag{18}$$

if using Gauss-Jordan elimination for the matrix inverse.

This measure is not the full number of computations that must occur to compute the electrostatic force or torque, but is the most time-intensive step. All other steps will involve the number of points and spheres in both models and are therefore more difficult to include without introducing unnecessary complexity.

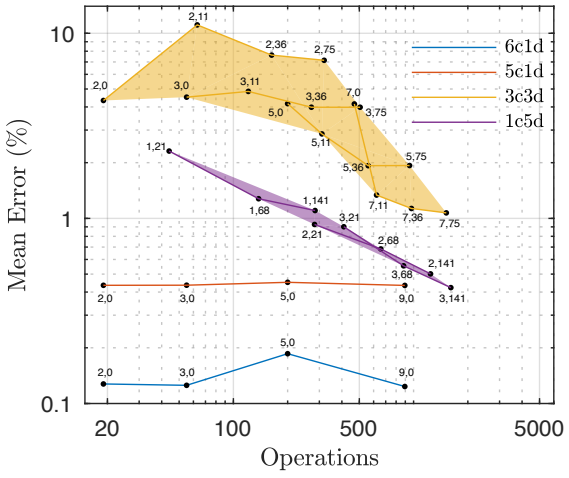

Fig. 11. Mean error for all spacecraft as a function of arithmetic operations

The mean error function is plotted in Fig. 11 for all spacecraft and all models as a function of operations, which are a proxy of computer time. The small numbers indicate which model is used – a pair of i, j indicates a model with i spheres and j points, and the color indicates the spacecraft. For the 6c1d and 5c1d spacecraft, only the conductor-only solution is shown since the others have poor performance. For the other two spacecraft, all the designs are shown with lines indicating models with the same number of spheres. Additionally, a boundary line and shading is used to indicate the likely Pareto front.

It is now clear that the 3c3d spacecraft is the least accurate, but still has mean error below 10% for all but one design. The 1c5d spacecraft follows a much tighter boundary and is more accurate while requiring roughly the same computational effort. Lastly, the two conductor only spacecraft are not strong functions of the computational effort but are very accurate no matter which model is used. This plot, or others like it, could be used to decide which model to use for a particular mission with known accuracy and speed constraints.

9. Conclusions

This paper seeks to answer two question: first, "when ought dielectrics be modeled?" and second, "how can dielectrics be modeled in MSM?". The first question is answered through an analysis of the mutual dielectric capacitance, and by including and neglecting dielectrics for certain models. For the four spacecraft analyzed, two of them do not need to have their dielectric components modeled. In fact, including them makes the solution worse. For the other two, ignoring dielectrics can lead to errors in the E field of 100s of percent. The mutual dielectric capacitance analysis provides the tools to extend this to other spacecraft than the four analyzed.

The second question is answered by using a point charge model for the dielectric portions of the spacecraft. When optimizing the full model, the points are included, but not allowed to be varied and 3 datasets that include a conductor only, mixed, and dielectric only case are included. Constraints can help enforce the far-field behavior without hurting the overall performance for some models, but the constraints are not always compliant for all models and all spacecraft. When optimized without any constraints, the predicted E field only differs from the truth model by less than 10%, often less than 1%. The conductor solutions are the most accurate, with the 1c5d and 3c3d following behind. Overall, modeling dielectrics using MSM is feasible and the errors for the cases considered here are less than other errors expected in the system.

References

[1] R. C. Olsen, "The record charging events of ats-6," *Journal of Spacecraft and Rockets*, vol. 24, no. 4, pp. 362–366, 1987.

[2] C. Früh, D. Ferguson, C. Lin, and M. Jah, "The effect of passive electrostatic charging on near-

geosynchronous high area-to-mass ratio objects," in *Proc. AAS Space Flight Mechanics Meeting*, Santa Fe, NM, Febuary 2014, pp. 3121–3137.

[3] J. Hughes and H. Schaub, "Rapid charged geosynchronous debris perturbation modeling of electromagnetic disturbances," in *AAS Spaceflight Mechanics Meeting*, Feb 5–9 2017.

[4] S. N. Paul and C. Früh, "Space debris charging and its effect on orbit evolution," *Journal of Guidance, Control, and Dynamics*, vol. 0, pp. 1–19, 2017.

[5] J. Hughes and H. Schaub, "Space weather influence on electromagnetic geosynchronous debris perturbations using statistical fluxes," *AGU Space Weather*, vol. 16, no. 4, pp. 391–405, 2018.

[6] J. Berryman and H. Schaub, "Analytical charge analysis for 2- and 3-craft coulomb formations," *AIAA Journal of Guidance, Control, and Dynamics*, vol. 30, no. 6, pp. 1701–1710, Nov.–Dec. 2007.

[7] E. Hogan and H. Schaub, "Collinear invariant shapes for three-craft coulomb formations," *Acta Astronautica*, vol. 12, pp. 78–89, March–April 2012.

[8] R. Inampudi and H. Schaub, "Optimal reconfigurations of two-craft coulomb formation in circular orbits," *AIAA Journal of Guidance, Control, and Dynamics*, vol. 35, no. 6, pp. 1805–1815, Nov. – Dec. 2012.

[9] H. Schaub and D. F. Moorer, "Geosynchronous large debris reorbiter: Challenges and prospects," *The Journal of the Astronautical Sciences*, vol. 59, no. 1–2, pp. 161–176, 2014.

[10] T. Bennett and H. Schaub, "Touchless electrostatic three-dimensional detumbling of large geo debris," in *AAS/AIAA Spaceflight Mechanics Meeting*, Jan. 26–30 2014.

[11] T. Bennett, D. Stevenson, E. Hogan, L. McManus, and H. Schaub, "Prospects and challenges of touchless debris despinning using electrostatics," *Advances in Space Research*, vol. 56, no. 3, pp. 557–568, 2015.

[12] T. Bennett and H. Schaub, "Capitalizing on relative motion in electrostatic detumbling of axi-symmetric geo objects," in *6th International Conference on Astrodynamics Tools and Techniques (ICATT)*, Darmstadt, Germany, March 14–17 2016.

[13] E. Hogan and H. Schaub, "Relative motion control for two-spacecraft electrostatic orbit corrections," *AIAA Journal of Guidance, Control, and Dynamics*, vol. 36, no. 1, pp. 240–249, Jan. – Feb. 2013.

[14] W. C. Gibson, *The method of moments in electromagnetics*. Chapman & Hall, November 28 2007.

[15] J. Q. Feng, "Electrostatic interaction between two charged dielectric spheres in contact," *Physical Review E*, vol. 62, no. 2, 2000.

[16] D. Stevenson and H. Schaub, "Multi-sphere method for modeling electrostatic forces and torques," *Advances in Space Research*, vol. 51, no. 1, pp. 10–20, Jan. 2013.

[17] P. Chow, J. Hughes, T. Bennett, and H. Schaub, "Automated sphere geometry optimization for the volume multi-sphere method," in *AAS/AIAA Spaceflight Mechanics Meeting*, Feb. 14–18 2016.

[18] G. Ingram, J. Hughes, T. Bennett, C. Reily, and H. Schaub, "Autonomous volume multi-sphere-model development using electric field matching," in *AAS Spaceflight Mechanics Meeting*, Feb 5–9 2017.

[19] J. Hughes and H. Schaub, "Effects of charged dielectrics on electrostatic force and torque," in *International Workshop on Spacecraft Formation Flying*, 2017.

[20] J. D. Jackson, *Classical Electrodynamics*. John Wiley & Sons, 1999.

[21] J. Lekner, "Electrostatics of two charged conducting spheres," *Procedings of the Royal Society*, vol. 468, pp. 2829–2848, 2012.

[22] P. Metzger and J. Lane, "Electric potential due to a system of conducting spheres," *The Open Applied Physics Journal*, vol. 2, pp. 32–48, 2009.

[23] J. Hughes and H. Schaub, "Spacecraft electrostatic force and torque expansions yielding appropriate fidelity measures," in *AAS Spaceflight Mechanics Meeting*, San Antonio, TX, Feb. 5–9 2017.